Biochemistry and Biophysics Reports 26 (2021) 101000

Contents lists available at ScienceDirect

Biochemistry and Biophysics Reports

journal homepage: www.elsevier.com/locate/bbrep

Plasmodium falciparum DDX17 is an RNA helicase crucial for parasite development

Suman Sourabh [a], Manish Chauhan [a], Rahena Yasmin [a], Sadaf Shehzad [b], Dinesh Gupta [b], Renu Tuteja [a,*]

[a] Parasite Biology Group, ICGEB, P. O. Box 10504, Aruna Asaf Ali Marg, New Delhi, 110067, India
[b] Translational Bioinformatics Group, ICGEB, P. O. Box 10504, Aruna Asaf Ali Marg, New Delhi, 110067, India

ARTICLE INFO

Keywords:
Artemisinin combination therapies (ACT)
Ded1
Helicase
Malaria
Plasmodium falciparum

ABSTRACT

Malaria is one of the major global health concerns still prevailing in this 21st century. Even the effect of artemisinin combination therapies (ACT) have declined and causing more mortality across the globe. Therefore, it is important to understand the basic biology of malaria parasite in order to find novel drug targets. Helicases play important role in nucleic acid metabolism and are components of cellular machinery in various organisms. In this manuscript we have performed the biochemical characterization of homologue of DDX17 from *Plasmodium falciparum* (PfDDX17). Our results show that PfDDX17 is an active RNA helicase and uses mostly ATP for its function. The qRT-PCR experiment results suggest that PfDDX17 is highly expressed in the trophozoite stage and it is localised mainly in the cytoplasm and in infected RBC (iRBC) membrane mostly in the trophozoite stage. The dsRNA knockdown study suggests that PfDDX17 is important for cell cycle progression. These studies report the biochemical functions of PfDDX17 helicase and further augment the fundamental knowledge about helicase families of *P. falciparum*.

1. Introduction

Malaria, an infectious disease, caused by the *Plasmodium* parasite is responsible for infecting millions across the globe even in the 21st century [1]. Five species of Plasmodium are known to cause malaria, *P. malariae*, *P. ovale*, *P. vivax*, *P. falciparum*, and *P. knowlesi*, among which *P. falciparum* has the most deleterious effect on human body [2]. The world malaria cases are almost same in 2016 and 2017 [3,4]. Now a days, *Plasmodium falciparum* has developed resistance to the artemisinin even when combined with other drugs like lumefantine, amodiaquine, piperaquine, sulfadoxine-pyrimethamine and mefloquine [5]. So, with the increasing threat of *P. falciparum* resistant strains, there is an immediate need to understand the basic biology of the parasite and find alternate drug targets.

Helicases are motor proteins having the ability to unwind the DNA or dsRNA into single strand by deriving energy from ATP hydrolysis [6]. Depending on the substrate, they can be classified as DNA or RNA helicases. On the basis of the conserved motifs, helicases are divided into six super families (SF1-SF6) [7]. Large number of RNA helicases are classified under SF2 which is further subdivided into three subfamilies as DEAD, DEAH and DExD/H box proteins hence making the SF2 as the largest superfamily. Furthermore, DEAD box helicases are sub categorised into groups like eIF4A, Has1, Rrp3 and Ded1 [8]. Recently, proteome analysis of *P. falciparum* showed that helicases, mainly DEAD-box proteins, can be promising anti-malarial drug targets [9].

Genome wide in-silico studies reported that there are seven members of Ded1 family of helicases in *P. falciparum* [8]. One of the members of Ded1 family known as PfDH60 (homologue of DDX5 or p68) has been characterised and reported to exhibit both DNA and RNA helicase activity. In case of DNA it is bipolar i.e., it exhibited unwinding in both 5′ to 3′ direction and 3′ to 5’ direction [10]. Also, the DNA helicase and ATPase activities are stimulated after phosphorylation of PfDH60 by PKC and it may be involved in DNA replication pathway in *P. falciparum* [10]. PfDH60 homologue in human named as DDX5 (Dead-box 5)/p68 shows only RNA helicase activity [11] and PKC phosphorylation inhibits ATPase and helicase activity [12]. Here we have reported detailed study on one of the members of Ded1 family from *P. falciparum* named DDX17 (PfDDX17) (PF3D7_1445900) which is a homologue of human DDX17 (p72) and Dbp2p from *Saccharomyces cerevisiae* [13,14]. The purified recombinant PfDDX17 shows DNA and RNA dependent ATPase activity

* Corresponding author.
E-mail addresses: renu@icgeb.res.in, renututeja@gmail.com (R. Tuteja).

https://doi.org/10.1016/j.bbrep.2021.101000
Received 29 December 2020; Received in revised form 9 March 2021; Accepted 7 April 2021

and it exhibits only RNA helicase activity. The results further show that for RNA helicase activity, PfDDX17 prefers mostly ATP for its function. The qRT-PCR results suggest that PfDDX17 is highly expressed in the trophozoite stage of intraerythrocytic development of parasite. The immunofluorescence studies revealed that PfDDX17 is localised mainly in the cytoplasm and on iRBC membrane mostly in the trophozoite stage. The dsRNA knockdown study suggests that PfDDX17 is most likely involved in cell cycle progression in the parasite.

2. Materials and methods

2.1. In silico analysis, structure modelling and docking

The amino acid sequence of PfDDX17 (PF3D7_ 1445900) was retrieved from the PlasmoDB v (9.2) (https://www.plasmodb.org) [15] and schematic diagram for its domains was predicted by using Scan-Prosite (http://prosite.expasy.org/prosite.html) [16]. The homologs were searched by NCBI blast using BLOSUM 62 and used for multiple sequence alignment using Clustal omega (https://www.ebi.ac.uk/Tools/msa/clustalo/) [17]. The orthologs of PfDDX17 were retrieved by ORTHOMCL-DB (ID: OG6_100364) (https://orthomcl.org/orthomcl/app) [18] and subjected to phylogenetic analysis using MEGAX [19].

For structure modelling, template exhibiting 84% query coverage and 54.73% identity used was 6UV0, ATP dependent RNA helicase of *Homo sapiens* [20]. The homology model was developed using PRIME with 6UV0 as template and loop refinement as suggested by Schrodinger [21]. The modelled structure was then subjected to molecular dynamics simulation of 10 ns for further validation using Desmond [22]. The Ramachandran plot was generated using RAMPAGE (http://mordred.bioc.cam.ac.uk/~rapper/rampage.php). The ADP was docked with PfDDX17 using FLARE version 3.0 [23]. The 13/39 RNA duplex was prepared using online server SimRNAweb (https://genesilico.pl/SimRNAweb/), a method for RNA 3D structure modelling [24]. Protein docking of complex PfDDX17-ADP with duplex 13/39 RNA was done using PIPER [25].

2.2. Cloning of PfDDX17 gene and protein expression

PfDDX17 gene has one intron of 1297 bp so, cDNA was used to amplify the gene using the forward and reverse primer, PfDDX17F (*Bam*HI site at the 5′ end) and PfDDX17R (*Xho*I site at the 3' end) (Supplementary table 1). The amplified PCR product was ligated in the cloning vector pJET 1.2 (Thermofischer Scientific Inc., USA) and transformed into DH10β *E. coli* cells. The gene was then transferred in to expression vector pET28a+. The gene PfDDX17 in pET28a+ was sequenced (Macrogen, Seoul, Korea) and sequence was submitted to NCBI database and GenBank accession number is MG879020.

The sequenced PfDDX17-pET28a + clone was transformed in BL21 (DE3) expression competent cells strain of *E. coli* for protein production. 2% of the overnight incubated primary culture was used for the secondary culture in Luria-Bertani media (Difco) with 0.1% chloramphenicol, 0.1% kanamycin and 3% ethyl alcohol. The secondary culture was grown till the OD reached to 0.8 at 37 °C then 1 mM IPTG was added for the protein induction and the culture was incubated at 16 °C for 18 h. For the suspension and maximum sonication of the culture pellet, lysis buffer of pH 7.5 (50 mM Tris-HCl, 500 mM NaCl, 0.05% Tween 20, 0.1% Triton X100 and 1 mM PMSF) was used followed by centrifugation at 10000 RPM at 4 °C for 30 min. The supernatant was allowed to bind with Ni-NTA (Qiagen, Germany) in a column equilibrated with the binding buffer (50 mM Tris-HCl pH 7.5, 200 mM NaCl and 20 mM imidazole) at 4 °C for 2 h in the presence of 20 mM imidazole to prevent non-specific binding. The column was washed with 200 ml of wash buffer (50 mM Tris pH 7.5, 200 mM NaCl and 50 mM imidazole) to remove impurities. The protein was eluted using different concentration of imidazole in cold elution buffer (50 mM Tris-HCl pH 7.5 and 200 mM NaCl). SDS-PAGE and Western blot analysis were done to check the purity of the recombinant PfDDX17. Western blot was done using His-tagged antibody conjugated with horse radish peroxidase (Sigma Aldrich, USA).

2.3. ATPase assay

The γ-^{32}P ATP was used for the detection of ATPase activity by measuring the release of free Pi. The purified protein was mixed with ATPase buffer (20 mM Tris–HCl, pH 8.0, 8 mM DTT, 1.0 mM $MgCl_2$, 20 mM KCl, and 16 μg/ml BSA) and mixture of ~17 nM of γ-^{32}P ATP and 1 mM of non-radioactive ATP and the reaction mixture was incubated at 37 °C for 1 h. For the DNA dependent and RNA dependent ATPase activity assay, 50 ng of M13mp19 ssDNA or 50 ng of RNA (RNA from P. falciparum trophozoite stage) were added to the above reaction. After an hour of incubation, the reaction was stopped by placing the eppendorf tube on ice and then 1 μl of the reaction mixture was loaded on the TLC membrane (Millipore, Germany). The hydrolysed Pi was separated by using the TLC buffer and then air-dried TLC membrane was exposed overnight to phosphor screen and scanned with phosphor imager. The graphical quantification was done using Image J software (http://rsbweb.nih.gov/ij/) [26]. Each experiment was done in duplicate.

2.4. Helicase substrate and helicase assays

DNA and RNA helicase substrates were prepared by using previously described methods [27,28]. The DNA and RNA sequences used for substrate preparation are given in the supplementary table no.2. For the DNA helicase assay, the total reaction volume of 10 μl contained purified recombinant protein, helicase buffer (20 mM Tris–HCl (pH 8.0), 8 mM DTT, 1.0 mM $MgCl_2$, 1.0 mM ATP, 10 mM KCl, 4% (w/v) sucrose, 80 μg/ml BSA) and γ-^{32}P labelled DNA substrate (1000 cpm/10 μl). The reaction mixture was incubated at 37 °C for 1 h and then the reaction was stopped by using the helicase dye (0.3% SDS, 10 mM EDTA, 10% Ficoll and 0.03% bromophenol blue). The mixture was then loaded and electrophoresed on 12% TBE gel for the separation of unwound ss and ds DNA. The gel was transferred for autoradiography and quantification was done using ImageJ software. The same method was used for RNA helicase assay by using RNA substrate in the place of DNA substrate. Each experiment was done in duplicate.

2.5. Immuno-fluorescence assay

To analyse the localization of the PfDDX17, thin smears of different blood stages of parasites were made and fixed using cold methanol at −80 °C for 15 min. The slides were then blocked using 3% bovine serum albumin (BSA) in 1X phosphate buffer saline (PBS) at 4 °C overnight. The slides were then washed in 1X PBS three times and allowed to bind with anti-PfDDX17 antibodies (developed in rabbit) at 1:250 dilutions in 1X PBS for 2 h at room temperature. After the incubation, the slides were washed three times with PBST (1XPBS with 0.5% Tween 20) and two times with 1X PBS (5 min each) to remove the non-specific binding. After washing the slides were incubated with secondary antibody and Alexa 488 (Goat anti-rabbit IgG secondary antibody) (Thermo Fisher Scientific) in 1:500 dilution (in 1X PBS) for 1 h at room temperature. At the end, slides were washed three times with PBST and two times with 1X PBS and mounted with 4,6-diamidino-2- phenylindole (DAPI) (Life Technologies, CA, USA). The prepared slides were visualised under Bio-Rad 2100 laser-scanning microscope attached to a Nikon TE 2000U microscope.

2.6. Synthesis of cDNA and quantitative RT-PCR

Synchronised culture was used to isolate RNA from three stages (ring, trophozoite and schizont) of *P. falciparum* 3D7 strain by using the RNeasy mini kit (Qiagen, Germany). The total RNA isolated was then used to synthesize cDNA by using the cDNA synthesis kit (Invitrogen,

USA). The cDNA prepared was then used for the Quantitative Real-Time PCR by using Fast SYBR Green qPCR master mix (Applied Biosystems, Life science Technology) and two pair of primer set for the detection of PfDDX17 (PfDDX17RTF and PfDDX17RTR) and 18s rRNA (18SF and 18SR) (primer no. 3,4,5 and 6 in supplementary table no. 1). Real time data analysis was done by comparing the PfDDX17 expression level with 18sRNA housekeeping gene level by ΔΔ Ct method. Experiment was repeated three times.

2.7. dsRNA mediated parasite growth study

Synchronised parasite culture with 2% haematocrit and ~1% parasitemia were used for study. The synchronised parasite culture was diluted in RPMI medium and 20 μg of dsRNA was added to the diluted culture and mixture was aliquoted in 96-well plates and incubated at 37 °C. The slides were prepared with 24 h gap up to 96 h (4 time points) and stained with Giemsa for the parasitemia counting and also smeared slides were used for immunofluorescence microscopy using anti-PfDDX17 antibody along with DAPI. The experiment was repeated three times.

3. Results

3.1. In-silico analysis

PfDDX17 is homologous to DDX17 (human) and Dbp2p (yeast), respectively [8]. The gene is 2881 base pairs, which includes a stretch of an intron of 1297 base pairs, and codes for a protein of ~60 kDa consisting of an ATPase domain and a helicase domain. The N-terminal has141 amino acids, the core region 312 amino acids constituting the ATPase domain and helicase domain, and the C-terminal has 74 amino acids. The multiple sequence alignment analysis of PfDDX17 with *H. sapiens* DDX17 and *S. cerevisiae* Dbp2p showed that PfDDX17 shares five most conserved motifs i.e., Q-motif, I, Ia, II and III with both the species. Interestingly, the core region contains 312 amino acids in *P. falciparum*, *H. sapiens* and *S. cerevisiae* (Supplementary Fig. 1). The diagrammatic representation of the motifs with their representative amino acids are also shown (Supplementary Fig. 2A). The PfDDX17 and the orthologous sequences from various *Plasmodium* species were subjected to MEGAX for phylogenetic analysis. The phylogenetic analysis revealed that within the Plasmodium genus, species *P. reichenowi* and *P. relictum* clustered together with the PfDDX17 exhibiting its more closeness with the two species, however the second cluster was formed among the species *P. knowlesi* and *P. vivax*. The third cluster consisted of Plasmodium species viz., *P. yoelii* and *P. berghei* along with the *S. cerevisiae* and *H. sapiens*, though the *P. malariae* and *P. ovale* always clustered separately (Supplementary Fig. 2B).

3.2. Purification of recombinant PfDDX17

The protein expression was done in BL21 (DE3) *E. coli* cells at 16 °C for 18 h. The purification was done by using Ni-NTA affinity chromatography and purity was checked by SDS PAGE analysis (Fig. 1A, lanes 1–4). The confirmation of the recombinant protein was done by Western blot analysis using anti-His monoclonal antibody (Fig. 1B, lanes 1 and 2) (Supplementary Fig. 3A and B). The pure fractions were stored at −80 °C and were used for different experiments and generation of polyclonal antibodies in rabbit.

3.3. ATPase assay

ATPase activity in case of DNA as the cofactor is quite low showing ~4% hydrolysis when the concentration of protein is 10 nM and gradually increases up to ~30% hydrolysis when 100 nM of protein was used (Fig. 1C, lanes 1–5 and Fig. 1D). With RNA as the cofactor, PfDDX17 shows ~20% hydrolysis in 10 nM protein and it linearly increases and saturates at ~45% hydrolysis at 100 nM of protein (Fig. 1C, lanes 6–10 and Fig. 1D). For time dependent ATPase activity 20 nM of PfDDX17 was used. In case of DNA, it showed ~5% ATP hydrolysis in 10 min and maximum hydrolysis of ~21% in 40 min (Fig. 1E, lanes 1–5 and Fig. 1F). When RNA was used as cofactor, PfDDX17 showed ~14% hydrolysis at 10 min and ~27% hydrolysis at 40 min (Fig. 1E, lanes 6–10 and Fig. 1F).

3.4. DNA and RNA helicase assay

The DNA and RNA duplex substrates were prepared using method described previously (Supplementary Fig. 4A and B; Supplementary table 2) [28]. With DNA duplex as substrate, no helicase activity was detected even at high concentration of PfDDX17 (Supplementary Fig. 4C). When RNA duplex substrate was used, PfDDX17 showed significantly strong helicase activity by unwinding ~30% of RNA substrate at 20 nM of protein concentration, ~55% unwinding at 60 nM and maximum at 100 nM i.e., ~79% unwinding (Fig. 1G lanes 1–5 and Fig. 1H). For time-dependent RNA helicase activity of PfDDX17, 20 nM of protein was used and the reaction was incubated at different time intervals from 0 to 20 min. The 15 min and 20 min reactions showed ~23% and ~25% unwinding of the substrate, respectively (Fig. 1I lanes 1–6 and Fig. 1J).

3.5. RNA helicase assay in presence of different dNTPs and NTPs

Different dNTPS and NTPs were used to study the RNA unwinding activity of PfDDX17 at a fixed concentration of 20 nM. The result revealed that ATP (Fig. 1K lane 8 and Fig. 1L) showed the maximum unwinding of ~24% followed by UTP and CTP (Fig. 1K and L).

3.6. Molecular docking

Human DDX17 exhibited 54.73% identity with PfDDX17 with about 84% coverage (Supplementary Fig. 5). The important nine motifs in PfDDX17 are highlighted in Fig. 2A. After dynamics simulation of 10 ns using Desmond PfDDX17 was docked with ADP using Flare version 3.0 taking into account the entire protein for grid generation. The Ramachandran plot, RMSD and radius of gyration are provided in supplementary Fig. 6B, supplementary Fig. 7A and B. The best binding pose predicted the LF dG (binding energy) of −4.411. The visualisation of the interacting residues of PfDDX17 with ADP exhibited the H-bonds with Lys-427 and Val-429 along with the hydrophobic interactions with Leu-424 (motif-V), Asp-425 (motif-V), Ile-426, Val-432, Thr-451, Lys-430, Arg-450 (motif-VI) and Arg-453 (motif-VI) (Fig. 2B). The interaction plot using LIGPLOT version 4.5.3 are also provided in supplementary Fig. 8A. PfDDX17-ADP complex and 13/39 RNA were docked using PIPER with 70000 ligand rotations to probe and 30 refined poses were returned and every pose was visualised using PyMol version 4.6.0 and in almost every pose the RNA was found to be docked within the same pocket in the helicase domain (Fig. 2C and D). The residues contributing to interactions were found to be Thr-88, Lys-89, Thr-373, Arg-381, Pro-386, Ala- 387, Leu-388, Cys-389, Lys-394, Lys-395, Glu-396, Glu-397, Arg-398, Arg-399, Trp-400, Leu-402, Asn-403, Glu-404, Lys-410, Ser-411, Ala-420 and Arg-422.

3.7. Localization of PfDDX17

To analyse the localization of the PfDDX17 immuno-fluorescence assay was done using anti-PfDDX17 antibody raised in rabbit with different intraerythrocytic developmental stages of *P. falciparum* 3D7 strain.

DAPI and fluorescent conjugated anti-rabbit antibody were used to detect nucleus and PfDDX17, respectively. In all the stages DDX17 is localised mainly in the cytoplasm. The expression of PfDDX17 is less in ring stage (Fig. 3B). During the trophozoite stage the expression level significantly increased and appeared on the iRBC membrane and

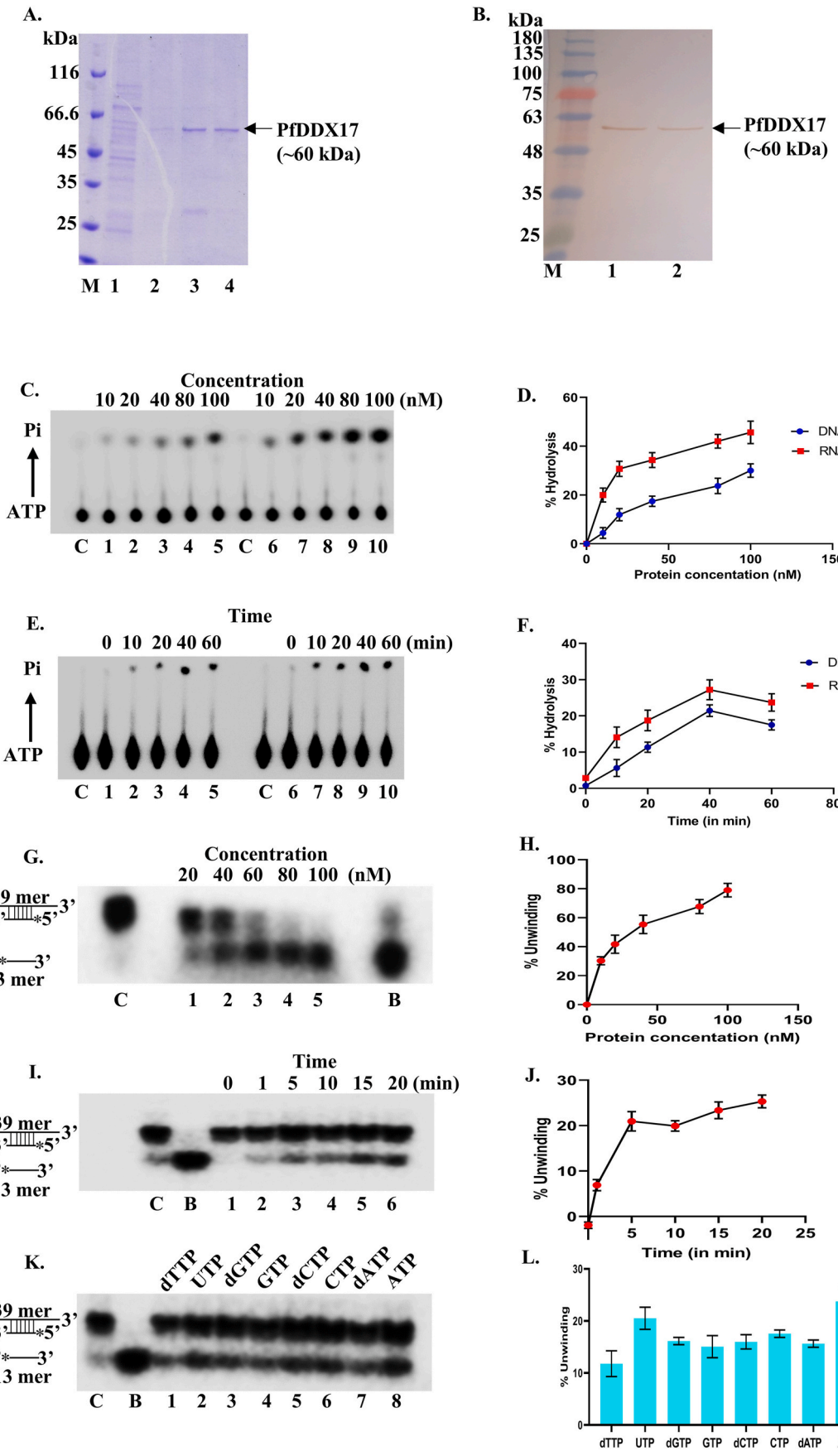

(caption on next page)

Fig. 1. Protein purification, ATPase and helicase assays
A. SDS-PAGE of PfDDX17. Lane M is marker, lane 1 is the wash fraction and lanes 2–4 are purified fraction of PfDDX17 (~60 kDa).
B. Western blot of PfDDX17. Lane M is marker and lanes 1 and 2 are PfDDX17 detected with anti-his antibody.
C. Concentration dependent ATPase activity of PfDDX17 using DNA and RNA as cofactor. C is control, lanes 1–5 show ATPase activity with increasing concentration of protein using DNA as cofactor and lanes 6–10 using RNA as cofactor.
D. The graphical presentation of the ATPase data.
E. Time dependent ATPase activity assay of PfDDX17 in the presence of DNA and RNA. Lanes 1–5 show the ATPase activity in the presence of DNA and lanes 6–10 shows the ATPase using RNA as cofactor.
F. Graphical illustration of the time dependent ATPase activity.
G. The RNA helicase activity with increasing concentration of PfDDX17 (lanes 1–5). Lane C is control and lane B is boiled substrate.
H. Quantitative analysis of the data.
I. Time dependent helicase activity of PfDDX17 (Lanes 1–6)
J. Graphical presentation of the time dependent helicase activity.
K. RNA helicase activity in the presence of different NTPS/dNTPS as mentioned in figure.
L. Quantitative analysis of the data.
Error bars represent standard deviation.

cytoplasm (Fig. 3D). Similar to the trophozoite stage PfDDX17 localised in the cytoplasm in the schizont and bursting schizont stage (Fig. 3E–F). The pre-immune serum did not detect DDX17 in the parasite (Fig. 3Ai-iii).

3.8. qRT-PCR analysis for gene expression

Total RNA of different parasite stages was isolated and used for qRT-PCR assay. The expression level of PfDDX17 was compared with 18s rRNA gene. The trophozoite stage shows the highest gene expression followed by ring and schizont stage (trophozoite > ring > schizont) (Fig. 3G). Also, the anti-PfDDX17 antibody detected the endogenous protein in the mixed parasite lysate using Western blot analysis (Supplementary Fig. 8B).

3.9. dsRNA mediated growth effect

To check the effect of PfDDX17 dsRNA on *P. falciparum* 3D7 growth, 1% parasitemia (sorbitol treated synchronised culture) and 2% haematocrit were used. The primer sequences and detailed steps of dsRNA preparation are presented in supplementary table 1 and supplementary Fig. 9A and B, respectively.

The green fluorescent protein (GFP) dsRNA was used as control. 20 μg/ml of PfDDX17 dsRNA and GFP dsRNA were used and the culture was observed for 96 h. The smears were prepared after every 24 h for Giemsa staining (counting parasitemia) and for immunofluorescence microscopy. The untreated culture did not show any changes and grew normally when observed till 96 h (Fig. 4 panel ii). Similarly, in GFP treated cells no significant changes were observed neither in cell cycle nor in morphological structure (Fig. 4). But in case of PfDDX17 dsRNA treated culture, there was cell cycle delay in ~72% of the infected cells (parasites were arrested in ring stage) (Fig. 4A iii and iv). Even after 48 h, PfDDX17 dsRNA treated cells were in late trophozoite or early schizont stage without showing any morphological change (Fig. 4B iii and iv). The observation at the end of 96 h showed that ~47% of the cells have delay in their cell cycle development in case of PfDDX17 whereas in GFP treated culture it was ~6% but no morphological changes or dead parasites were noticed (Fig. 4E). The immunofluorescence assay was done up to 48 h and it was observed that there is drastic change in the protein expression level in PfDDX17 dsRNA treated cells (Supplementary fig. 9C).

4. Discussion

In-silico analysis showed that the four motifs I, Ia, II and III of PfDDX17 are highly conserved and similar to *H. sapiens* DDX17 and *S. cerevisiae* Dbp2. Motif Ib has CPGR in *P. falciparum* but in human and yeast it is TPGR. Motif IV is different in all species, the *P. falciparum* contains IIV but in case of human and yeast it is TII and TLI, respectively. In motif V, *P. falciparum* and human share the common sequence RGLD but in yeast there is a substitution and leucine is changed to isoleucine (RGID). The last motif VI is common in *P. falciparum* and yeast (HRIGRTGR) and is changed to HRIGRTAR in human. From the ORTHOMCL-DB it was found that PfDDX17 is the ortholog of the human and yeast counterpart and it is evolutionary conserved in the *P. falciparum*, *H. sapiens* and *S. cerevisiae*. So, PfDDX17 did not show DNA helicase activity but its ATP dependent RNA helicase activity is conserved from higher taxa to lower. The structural modelling of PfDDX17 divided the nine motifs into two domains. The motifs Q, I, Ia, Ib, II and III constitute the ATPase domain and IV, V and VI form the helicase domain. Similar to DOZI, PfDDX17 is also an RNA helicase but it unwinds maximum RNA at 80 nM concentration whereas DOZI exhibits maximum unwinding at 150 nM concentration [27]. The docking of the ADP at the amino acid Leu-424 and Asp-425 of motif V and Arg-450, Thr-451 and Arg-453 of motif VI showed the most conserved interaction with the NTP [29]. Helicases can utilize the energy derived from variety of NTPs for their unwinding activity [30]. PfDDX17 showed unwinding activity in all NTPs and dNTPs but showed maximum activity in presence of ATP. Also, previous studies have reported that PfWrn and PfUvrD helicases are able to use all types of NTPs and dNTPS for their unwinding activity [30,31].

The localization study showed that like DOZI, PfDDX17 localises mostly in the cytoplasm but it is interesting to note that PfDDX17 is detected on the iRBC membrane also. Maximum transcript level of DDX17 was observed in trophozoite stage of intraerythrocytic development in *P. falciparum* 3D7 strain. The trophozoite stage is the most metabolically active stage of the *P. falciparum*. During this stage the regulation of most of the genes are at peak point and the parasite prepares for the production of daughter cells through mitosis [32]. It has been reported previously that PfDDX55 is also expressed maximally in the trophozoite stage [33]. But the transcript level of a gene in *P. falciparum* can vary in different intraerythrocytic stage and is not proportional to the content of DNA during the schizont stage [34]. The transcription and translation for a particular gene could be different in different stages of the parasite [32]. Previously, we have reported that gene expression of PfDDX31, ATP dependent DNA helicase, is more in schizont stage but the transcript level is more in ring stage [35].

After the invasion of merozoite into uninfected RBC the parasite stays in the ring stage for ~24 h. The stage i.e. trophozoite stage takes ~12 h and the shortest duration is schizont stage which is ~8 h. PfDDX17 dsRNA mediated knock down study in *P. falciparum* 3D7 strain showed that the dsRNA treatment caused the delay in the cell cycle by ~16 h. It has been reported that PfDDX17 is a part of phophoproteome in the cell cycle progression from ring to schizont stage [36]. Another similar study showed that PfDDX17 is a part of cell cycle regulatory system in *P. falciparum* [37]. It has been reported earlier that when the protein levels of p68 and p72 were reduced by RNA interference in mouse myoblast cells it affected the cell differentiation [38]. Recent

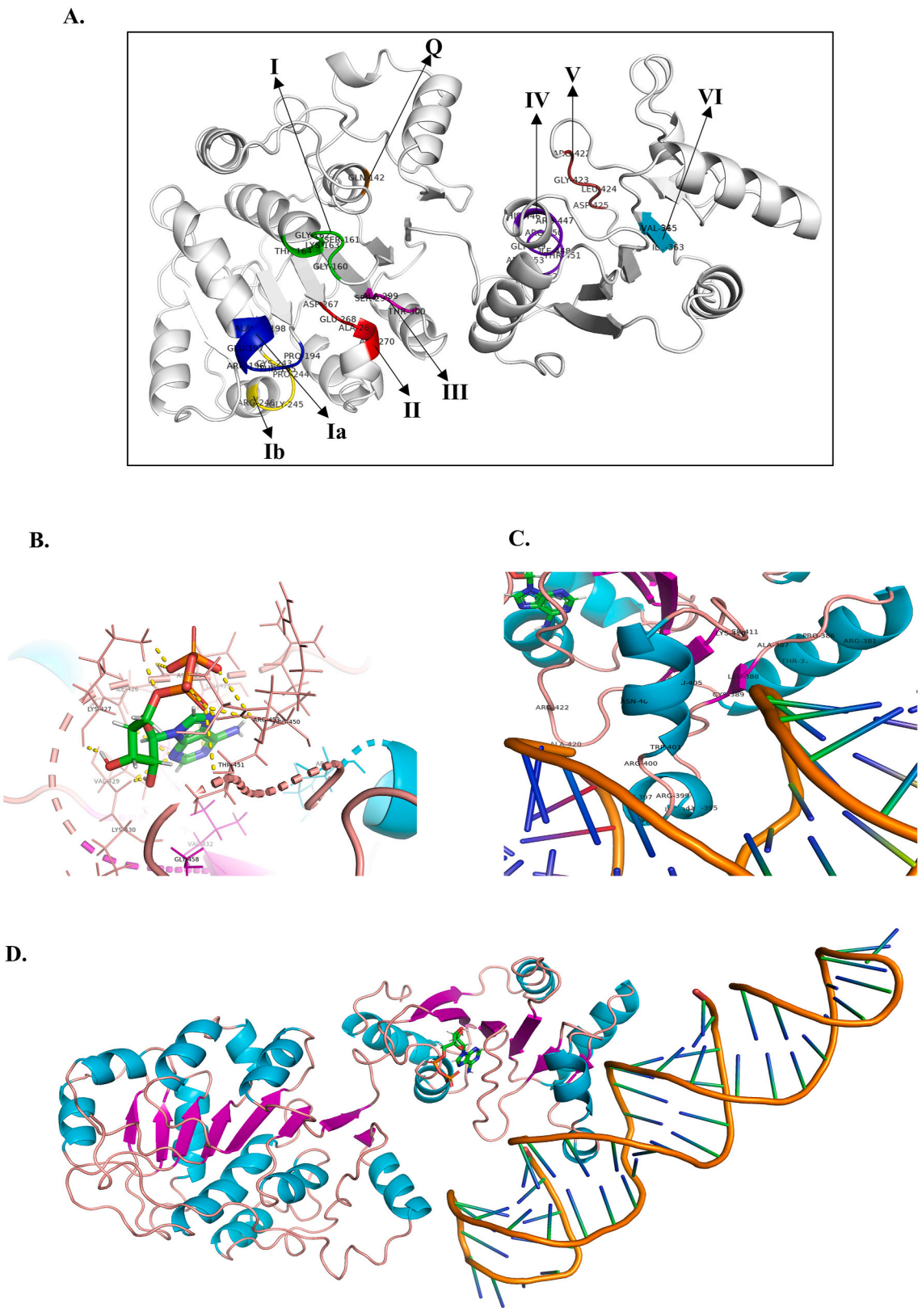

Fig. 2. Structural modelling and molecular docking of PfDDX17 with ADP and 13/39 mer RNA
A. Structure of PfDDX17 with 9 motifs: Motif Q (orange), motif I (green), motif Ia (blue) motif Ib (yellow), motif II (red), motif III (magenta), motif IV (cyan), motif V (firebrick) and motif VI (purple)are shown.
B. Interacting residues of PfDDX17 with ADP expanded around the 4 Å.
C. Interacting residues of PfDDX17-ADP complex with 13/39 RNA expanded around the 4 Å. **D.** Cartoon representation of PfDDX17-ADP (helix-sheet-loop) in a docked pose with 13/39 RNA. (For interpretation of the references to colour in this figure legend, the reader is referred to the Web version of this article.)

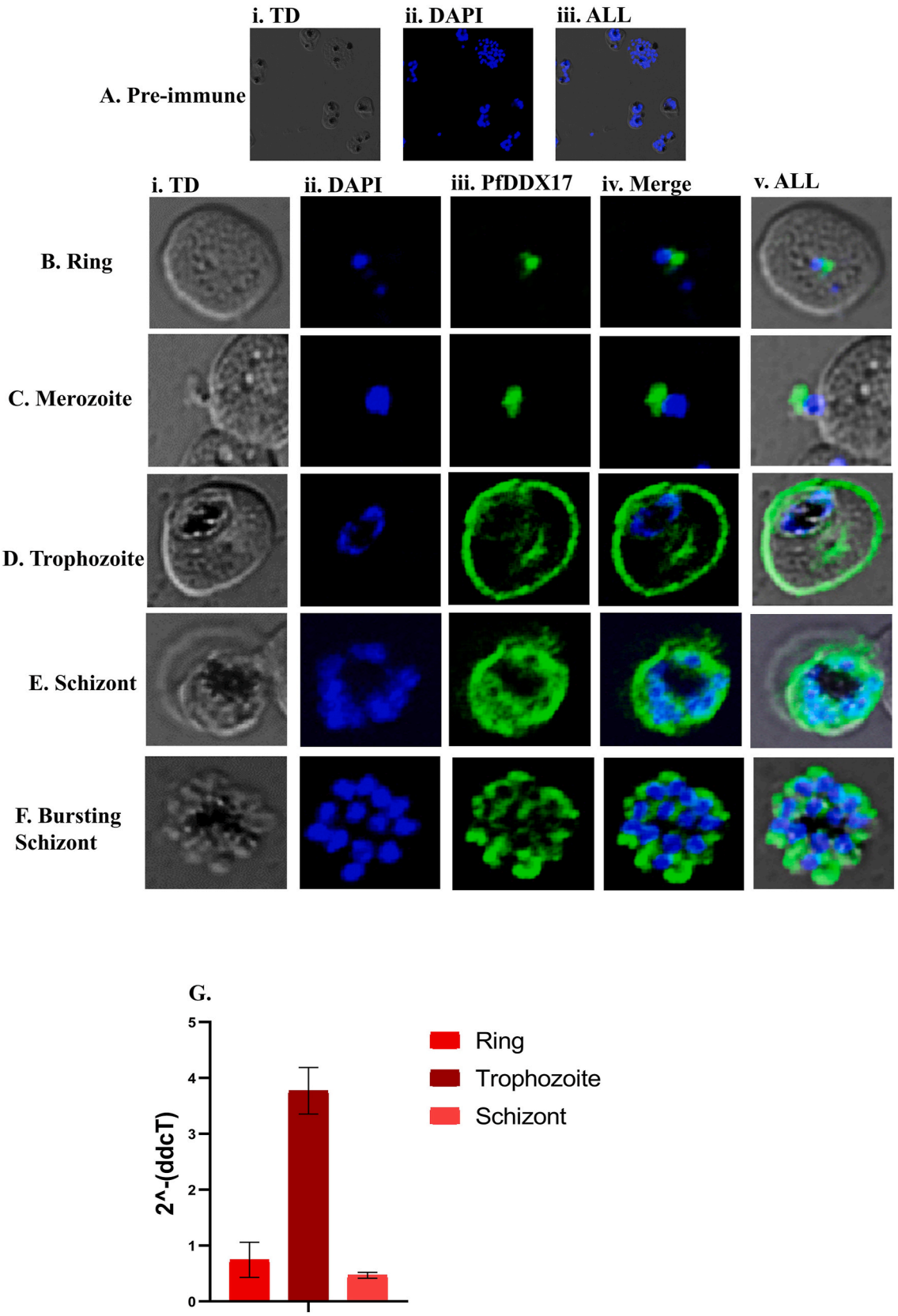

Fig. 3. Localization of PfDDX17

A. Preimmune staining (i) Phase contrast (TD); (ii) DAPI; (iii) All merged. **B.** Ring stage, **C.** Merozoite stage, **D.** Trophozoite stage, **E.** Schizont stage, **F.** Mature Schizont, (i) TD, (ii) DAPI, (iii) PfDDX17, (iv) merged (DAPI + PfDDX17). **G.** The transcript level of PfDDX17 of different intraerythrocytic stages of *P. falciparum* 3D7 strain using Real time PCR. Error bars represent standard deviation.

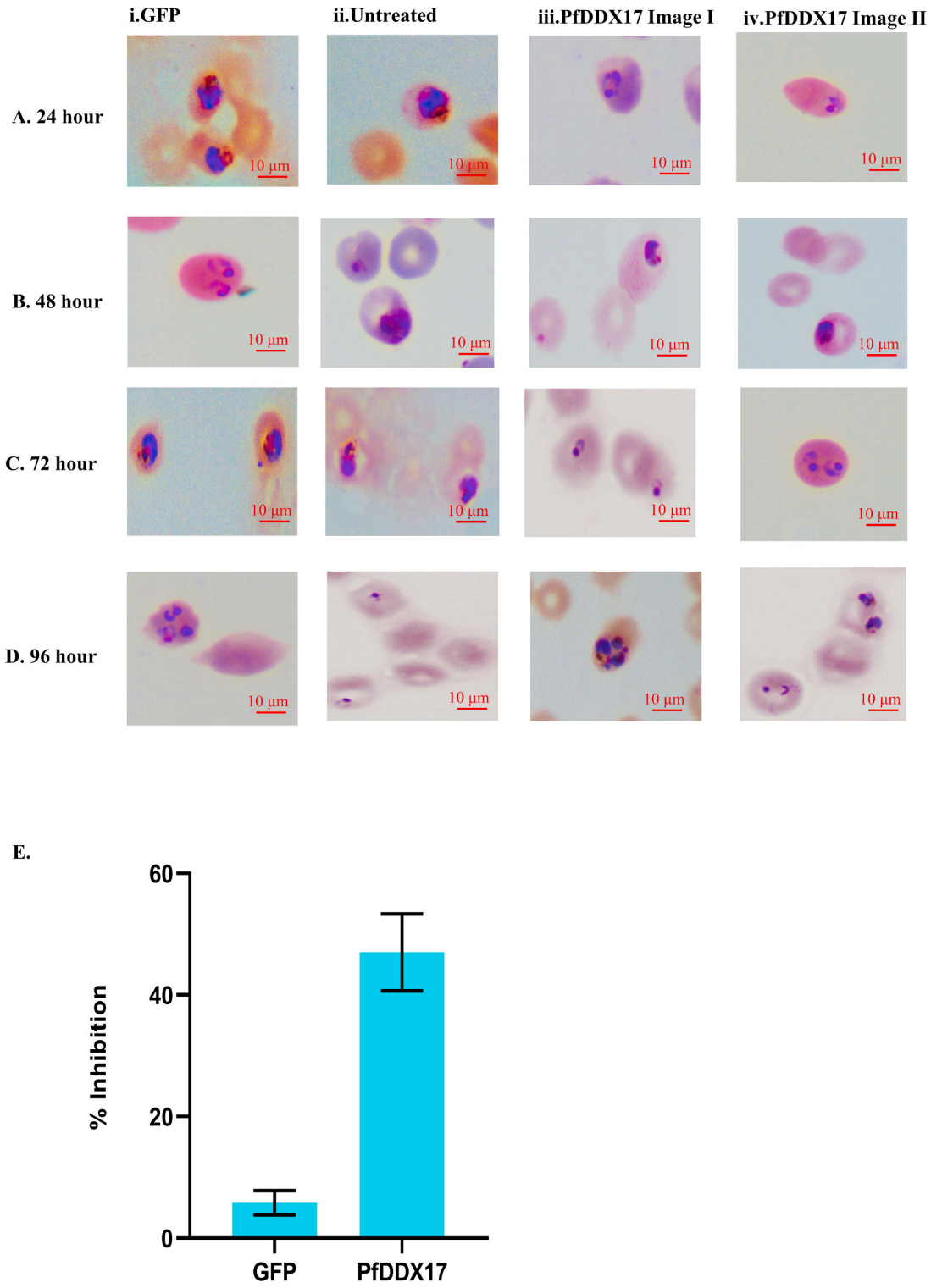

Fig. 4. Effect of dsRNA on parasite cell cycle up to 96 h. Panel i Giemsa stained images of GFP treated culture (control). Panel ii images of the untreated culture and panel iii and iv images of the PfDDX17 dsRNA treated culture **E.** Manually calculated percentage of parasite infected RBC undergoing delay in cell cycle at 96 h. Error bars represent standard deviation.

study showed that when the human DDX17 was knocked down in hepatocellular carcinoma (HCC), the HCC cell proliferation was inhibited [39]. In previous studies we have reported that the growth of *P. falciparum* 3D7 strain was inhibited when the parasite was treated with dsRNA of PfMLH [40], PfUvrD [41], PfBlm [42] and PSH2 [28]. In these studies, the morphological changes or dead parasites were visible after 48 h but in case of PfDDX17 no distortion of the parasite or cell death was noticed till the end of 96 h.

In this study, we have reported the detailed characterisation of the full-length PfDDX17 protein. Ded1 family member PfDH60 is dual helicase and expressed only in schizont stages [10]. In comparison, PfDDX17 is only an RNA helicase and expressed in all the intra-erythrocytic stages of development of *P. falciparum* 3D7 strain.

Declaration of competing interest

The authors declare that there is no conflict of interest.

Acknowledgments

The authors gratefully acknowledge the infrastructural support from the Department of Biotechnology, Government of India. Suman Sourabh is grateful to Council for Scientific and Industrial Research (CSIR), Government of India, for providing the fellowship.

Appendix A. Supplementary data

Supplementary data to this article can be found online at https://doi.org/10.1016/j.bbrep.2021.101000.

Author Statement

All authors certify that they have participated sufficiently in the work to take responsibility for the content, including participation in the concept, design, analysis, writing, or revision of the manuscript.

References

[1] J.G. Breman, A.D. Brandling-Bennett, The challenge of malaria eradication in the twenty-first century: Research linked to operations is the key, Vaccine 29 (2011) D97–D103, https://doi.org/10.1016/j.vaccine.2011.12.003.
[2] T.F. De Koning-Ward, M.W.A. Dixon, L. Tilley, P.R. Gilson, Plasmodium species: master renovators of their host cells, Nat. Rev. Microbiol. 14 (2016) 494–507, https://doi.org/10.1038/nrmicro.2016.79.
[3] WHO Report, World malaria report 2017. https://doi.org/10.1071/EC12504, 2017.
[4] WHO Report, WHO | the World malaria report 2018. https://www.who.int/malaria/publications/world-malaria-report-2018/, 2018.
[5] C. Nsanzabana, Resistance to artemisinin combination therapies (ACTs): do not forget the partner Drug!, Trav. Med. Infect. Dis. 4 (2019), https://doi.org/10.3390/tropicalmed4010026.
[6] S. Rocak, P. Linder, Dead-box proteins: the driving forces behind RNA metabolism, Nat. Rev. Mol. Cell Biol. 5 (2004) 232–241, https://doi.org/10.1038/nrm1335.
[7] M.R. Singleton, M.S. Dillingham, D.B. Wigley, Structure and mechanism of helicases and nucleic acid translocases, Annu. Rev. Biochem. 76 (2007) 23–50, https://doi.org/10.1146/annurev.biochem.76.052305.115300.
[8] R. Tuteja, Genome wide identification of Plasmodium falciparum helicases: a comparison with human host, Cell Cycle 9 (2010) 104–120, https://doi.org/10.4161/cc.9.1.10241.
[9] M. Dousti, R. Manzano-Román, S. Rashidi, G. Barzegar, N.B. Ahmadpour, A. Mohammadi, G. Hatam, A proteomic glimpse into the effect of antimalarial drugs on Plasmodium falciparum proteome towards highlighting possible therapeutic targets, Pathog. Dis. (2020) 1–18, https://doi.org/10.1093/femspd/ftaa071.
[10] A. Pradhan, V.S. Chauhan, R. Tuteja, Plasmodium falciparum DNA helicase 60 is a schizont stage specific, bipolar and dual helicase stimulated by PKC phosphorylation, Mol. Biochem. Parasitol. 144 (2005) 133–141, https://doi.org/10.1016/j.molbiopara.2005.08.006.
[11] H. Hirling, M. Scheffner, T. Restle, H. Stahl, RNA helicase activity associated with the human p68 protein, Nature 339 (1989) 562–564, https://doi.org/10.1038/339562a0.
[12] M.K. Buelt, B.J. Glidden, D.R. Storm, Regulation of p68 RNA helicase by calmodulin and protein kinase C, J. Biol. Chem. 269 (1994) 29367–29370.
[13] C.R. Nelson, T. Mrozowich, S.M. Park, S. D'souza, A. Henrickson, J.R.J. Vigar, H. J. Wieden, R.J. Owens, B. Demeler, T.R. Patel, Human DDX17 unwinds rift valley fever virus non-coding RNAs, Int. J. Mol. Sci. 22 (2021) 1–17, https://doi.org/10.3390/ijms22010054.
[14] Z. Xing, W.K. Ma, E.J. Tran, The DDX5/Dbp2 subfamily of DEAD-box RNA helicases, Wiley Interdiscip. Rev. RNA 10 (2019) e1519, https://doi.org/10.1002/wrna.1519.
[15] C. Aurrecoechea, J. Brestelli, B.P. Brunk, J. Dommer, S. Fischer, B. Gajria, X. Gao, A. Gingle, G. Grant, O.S. Harb, M. Heiges, F. Innamorato, J. Iodice, J.C. Kissinger, E. Kraemer, W. Li, J.A. Miller, V. Nayak, C. Pennington, D.F. Pinney, D.S. Roos, C. Ross, C.J. Stoeckert, C. Treatman, H. Wang, PlasmoDB: a functional genomic database for malaria parasites, Nucleic Acids Res. 37 (2009) 539–543, https://doi.org/10.1093/nar/gkn814.
[16] E. de Castro, C.J.A. Sigrist, A. Gattiker, V. Bulliard, P.S. Langendijk-Genevaux, E. Gasteiger, A. Bairoch, N. Hulo, ScanProsite: detection of PROSITE signature matches and ProRule-associated functional and structural residues in proteins, Nucleic Acids Res. 34 (2006) 362–365, https://doi.org/10.1093/nar/gkl124.
[17] F. Sievers, A. Wilm, D. Dineen, T.J. Gibson, K. Karplus, W. Li, R. Lopez, H. McWilliam, M. Remmert, J. Söding, J.D. Thompson, D.G. Higgins, Fast, scalable generation of high-quality protein multiple sequence alignments using Clustal Omega, Mol. Syst. Biol. 7 (2011), https://doi.org/10.1038/msb.2011.75.
[18] F. Chen, A.J. Mackey, C.J. Stoeckert, D.S. Roos, OrthoMCL-DB: querying a comprehensive multi-species collection of ortholog groups, Nucleic Acids Res. 34 (2006) D363–D368, https://doi.org/10.1093/nar/gkj123.
[19] S. Kumar, G. Stecher, M. Li, C. Knyaz, K. Tamura, X. Mega, Molecular evolutionary genetics analysis across computing platforms, Mol. Biol. Evol. 35 (2018) 1547–1549, https://doi.org/10.1093/molbev/msy096.
[20] T.D. Ngo, A.C. Partin, Y. Nam, RNA specificity and autoregulation of DDX17, a modulator of MicroRNA biogenesis, Cell Rep. 29 (2019) 4024–4035, https://doi.org/10.1016/j.celrep.2019.11.059, e5.
[21] M.P. Jacobson, D.L. Pincus, C.S. Rapp, T.J.F. Day, B. Honig, D.E. Shaw, R. A. Friesner, A hierarchical approach to all-atom protein loop prediction, Proteins Struct. Funct. Genet. 55 (2004) 351–367, https://doi.org/10.1002/prot.10613.
[22] K.J. Bowers, D.E. Chow, H. Xu, R.O. Dror, M.P. Eastwood, B.A. Gregersen, J. L. Klepeis, I. Kolossvary, M.A. Moraes, F.D. Sacerdoti, J.K. Salmon, Y. Shan, D. E. Shaw, Scalable algorithms for molecular dynamics simulations on commodity clusters, in: Institute of Electrical and Electronics Engineers (IEEE), 2007, https://doi.org/10.1109/sc.2006.54, 43–43.
[23] T. Cheeseright, M. Mackey, S. Rose, A. Vinter, Molecular field extreme as descriptors of biological activity: definition and validation, J. Chem. Inf. Model. 46 (2006) 665–676, https://doi.org/10.1021/ci050357s.
[24] M. Magnus, M.J. Boniecki, W. Dawson, J.M. Bujnicki, SimRNAweb: a web server for RNA 3D structure modeling with optional restraints, Nucleic Acids Res. 44 (2016) W315–W319, https://doi.org/10.1093/nar/gkw279.
[25] D. Kozakov, R. Brenke, S.R. Comeau, S. Vajda, PIPER: an FFT-based protein docking program with pairwise potentials, Proteins Struct. Funct. Genet. 65 (2006) 392–406, https://doi.org/10.1002/prot.21117.
[26] C.A. Schneider, W.S. Rasband, K.W. Eliceiri, NIH Image to ImageJ: 25 years of image analysis, Nat. Methods 9 (2012) 671–675, https://doi.org/10.1038/nmeth.2089.
[27] M. Tarique, M. Ahmad, A. Ansari, R. Tuteja, Plasmodium falciparum DOZI, an RNA helicase interacts with eIF4E, Gene 522 (2013) 46–59, https://doi.org/10.1016/j.gene.2013.03.063.
[28] M. Chauhan, R. Tuteja, Plasmodium falciparum specific helicase 2 is a dual, bipolar helicase and is crucial for parasite growth, Sci. Rep. 9 (2019) 1–15, https://doi.org/10.1038/s41598-018-38032-1.
[29] H. Ding, M. Guo, V. Vidhyasagar, T. Talwar, Y. Wu, The Q motif is involved in DNA binding but not ATP binding in ChlR1 helicase, PloS One 10 (2015) 1–22, https://doi.org/10.1371/journal.pone.0140755.
[30] M. Ahmad, A. Ansari, M. Tarique, A.T. Satsangi, R. Tuteja, Plasmodium falciparum UvrD helicase translocates in 3′ to 5′ direction, colocalizes with MLH and modulates its activity through physical interaction, PloS One 7 (2012), https://doi.org/10.1371/journal.pone.0049385.
[31] F. Rahman, M. Tarique, M. Ahmad, R. Tuteja, Plasmodium falciparum Werner homologue is a nuclear protein and its biochemical activities reside in the N-terminal region, Protoplasma 253 (2016) 45–60, https://doi.org/10.1007/s00709-015-0785-6.
[32] H.J. Painter, N.C. Chung, A. Sebastian, I. Albert, J.D. Storey, M. Llinás, Real-time in vivo global transcriptional dynamics during plasmodium falciparum blood-stage development, BioRxiv (2018) 265975, https://doi.org/10.1101/265975.
[33] R. Yasmin, I. Kaur, R. Tuteja, Plasmodium falciparum DDX55 is a nucleocytoplasmic protein and a 3′-5′ direction-specific DNA helicase, Protoplasma 257 (2020) 1049–1067, https://doi.org/10.1007/s00709-020-01495-z.
[34] N. Rovira-Graells, A.P. Gupta, E. Planet, V.M. Crowley, S. Mok, L.R. De Pouplana, P.R. Preiser, Z. Bozdech, A. Cortés, Transcriptional variation in the malaria parasite Plasmodium falciparum, Genome Res. 22 (2012) 925–938, https://doi.org/10.1101/gr.129692.111.
[35] R. Yasmin, M. Chauhan, S. Sourabh, R. Tuteja, Plasmodium falciparum DDX31 is DNA helicase localized in nucleolus, Heliyon 5 (2019), https://doi.org/10.1016/j.heliyon.2019.e02905.
[36] B.N. Pease, E.L. Huttlin, M.P. Jedrychowski, E. Talevich, J. Harmon, T. Dillman, N. Kannan, C. Doerig, R. Chakrabarti, S.P. Gygi, D. Chakrabarti, Global analysis of protein expression and phosphorylation of three stages of plasmodium falciparum intraerythrocytic development, J. Proteome Res. 12 (2013) 4028–4045, https://doi.org/10.1021/pr400394g.
[37] H. Cai, C. Hong, T.G. Lilburn, A.L. Rodriguez, S. Chen, J. Gu, R. Kuang, Y. Wang, A novel subnetwork alignment approach predicts new components of the cell cycle regulatory apparatus in Plasmodium falciparum, BMC Bioinf. 14 (2013) S2, https://doi.org/10.1186/1471-2105-14-S12-S2.
[38] G. Caretti, R.L. Schiltz, F.J. Dilworth, M. Di Padova, P. Zhao, V. Ogryzko, F. V. Fuller-Pace, E.P. Hoffman, S.J. Tapscott, V. Sartorelli, The RNA helicases p68/p72 and the noncoding RNA SRA are coregulators of MyoD and skeletal muscle differentiation, Dev. Cell 11 (2006) 547–560, https://doi.org/10.1016/j.devcel.2006.08.003.
[39] Y. Xue, X. Jia, C. Li, K. Zhang, L. Li, J. Wu, J. Yuan, Q. Li, DDX17 promotes hepatocellular carcinoma progression via inhibiting Klf4 transcriptional activity, Cell Death Dis. 10 (2019), https://doi.org/10.1038/s41419-019-2044-9.
[40] M. Tarique, M. Chauhan, R. Tuteja, ATPase activity of Plasmodium falciparum MLH is inhibited by DNA-interacting ligands and dsRNAs of MLH along with UvrD

curtail malaria parasite growth, Protoplasma 254 (2017) 1295–1305, https://doi.org/10.1007/s00709-016-1021-8.

[41] M. Tarique, F. Tabassum, M. Ahmad, R. Tuteja, Plasmodium falciparum UvrD activities are downregulated by DNA-interacting compounds and its dsRNA inhibits malaria parasite growth, BMC Biochem. 15 (2014) 1–10, https://doi.org/10.1186/1471-2091-15-9.

[42] F. Rahman, M. Tarique, R. Tuteja, Plasmodium falciparum Bloom homologue, a nucleocytoplasmic protein, translocates in 3′ to 5′ direction and is essential for parasite growth, Biochim. Biophys. Acta Protein Proteonomics 1864 (2016) 594–608, https://doi.org/10.1016/j.bbapap.2016.02.016.